symmetry

MDPI

*Article*

# Comparative Study: Catalytic Activity and Rhodamine Dye Luminescence at the Surface of $TiO_2$-Based Nanoheterostructures

**Elizaveta Konstantinova [1,2], Vladimir Zaitsev [1], Artem Marikutsa [3] and Alexander Ilin [1,*]**

1 Physics Department, Lomonosov Moscow State University, 119991 Moscow, Russia; konstantinova@physics.msu.ru (E.K.); zaytsev@physics.msu.ru (V.Z.)
2 Faculty of Nano-Bio-Information and Cognitive Technologies, Moscow Institute of Physics and Technology, 141700 Dolgoprudny, Moscow Region, Russia
3 Chemistry Department, Lomonosov Moscow State University, 119991 Moscow, Russia; artem.marikutsa@gmail.com
* Correspondence: as.ilin@physics.msu.ru; Tel.: +7-495-939-1666

**Abstract:** Nanoheterostructures based on titanium, molybdenum, tungsten, and vanadium nanooxides with symmetric crystal structures, morphologies and high photocatalytic activity in under illumination by visible light, have been synthesized and studied. Microscopy, optical spectroscopy, and electron-spin resonance techniques were used. The asymmetric separation of photo-generated holes and electrons between different nanooxides in their nanoheterostructures suppresses their recombination. Using the method developed by the authors and based on ESR spectroscopy, the energy levels of the active centers inside the band gaps of the studied samples were found. We have shown, for the first time, that under illumination of nanoheterostructures under asymmetric conditions with adsorbed rhodamine dye at the dye-absorption wavelength (500 nm), photocatalytic reactions are mainly determined by light absorption by the nanostructures themselves, and not by energy transfer from the dye. This important result shows that high photocatalytic activity of materials with symmetric crystal structures is the primary criterion for creating energy-efficient photocatalysts. The results will be useful for the development of energy-efficient catalytic devices based on various combinations of metal nanooxides.

**Keywords:** titanium dioxide; nanoheterostructures; adsorbed dye molecules; spin centers; photosensitivity; photocatalysis; symmetry



**Citation:** Konstantinova, E.; Zaitsev, V.; Marikutsa, A.; Ilin, A. Comparative Study: Catalytic Activity and Rhodamine Dye Luminescence at the Surface of $TiO_2$-Based Nanoheterostructures. *Symmetry* **2021**, *13*, 1758. https://doi.org/10.3390/sym13091758

Academic Editors: Sabino Armenise, Franck Launay and Marta Muñoz

Received: 12 August 2021
Accepted: 17 September 2021
Published: 21 September 2021



## 1. Introduction

In the few last decades many researchers have been focused on titanium dioxide, which exhibits unique properties [1–6] for gas sensorics [7], solar cells [1], and (most importantly) in the photo catalysis–photo-chemical decomposition of organic impurities (including toxic ones) on the $TiO_2$ surface [8–10]. Nanocrystalline titanium dioxide has a very developed, open-to-ambient-molecules surface with an area that varies, depending on the synthesis method, from tens to hundreds of square meters per gram of substance, and the highest photoactivity among all known metal oxides [11,12]. The driving force of photo catalysis (i.e., reduction/oxidation reactions) are radicals efficiently generated by light in $TiO_2$ due to adsorbed water and oxygen molecules' interaction at the surface with photoexcited charge carriers. The functional characteristics of $TiO_2$ are determined by its physicochemical properties. Titanium dioxide is a wide-gap semiconductor with a band gap from 3.2 to 3.4 eV, and continuous illumination by UV radiation must be used for the generation of reactive electrons and holes [7]. Numerous studies have shown that the doping with ions of metals or nonmetals (e.g., carbon and nitrogen) increases the light absorption coefficient in the visible spectral range, thus affecting the photocatalytic properties of $TiO_2$ [13–17]. Another way to improve photocatalytic efficiency is to

increase the lifetime of photoexcited carriers (holes and electrons) by their asymmetric spatial separation inside catalyst heterostructures, thus hampering recombination. In this case, continuous illumination is no longer necessary. To provide these conditions, $TiO_2$ is combined with symmetric semiconductor oxides of vanadium ($V_2O_5$), molybdenum ($MoO_3$), and tungsten ($WO_3$) [18–20].

In [20] we investigated the morphologies of nitrogen-doped $TiO_2$–based nanoheterostructures and the types of radicals within them, and found a correlation between the rate of photocatalysis and the concentration of radicals in the samples. In the present paper we have obtained nitrogen-doped $TiO_2$–based nanoheterostructures that symmetrically absorb visible light and accumulate photoexcited charge carriers, providing continuation of the catalytic activity of the produced structures for a rather long time after illumination is ceasedm, and, at the same time, we have thoroughly examined the behavior of the prepared nanoheterostructures after the adsorbtion of organic dye molecules on their surface. Organic dye molecules' adsorption is involved in the standard method for photocatalytic activity measurement. We have shown in the present work that the procedure of photocatalytic activity investigation involving rhodamine dye molecules is reliable and trustworthy. Additionally, we have measured the position of the energy levels of the active centers inside the band gaps of the $TiO_2$–based nanoheterostructures, using ESR spectroscopy to reveal the centers that can absorb light in the visible spectrum.

## 2. Materials and Methods

Nitrogen-doped nanostructured titanium dioxide and $TiO_2-MoO_3$, $TiO_2-V_2O_5$, $TiO_2-WO_3$, $TiO_2-MoO_3-WO_3$, and $TiO_2-MoO_3-V_2O_5$ nanoheterostructures were prepared by the sol-gel technique. Nanocrystalline nitrogen-doped titanium dioxide with symmetric structure was prepared by controlled hydrolysis through the dropwise addition of 12.5% $NH_4OH$ to 2.5-M $TiCl_4$ aqueous solution + 0.65-M HCl cooled to 0 °C with rigorous stirring until pH = 4 was reached. The obtained precipitate was washed with distilled water and dispersed with ultrasound. Next, the gel precipitate was annealed in a furnace at 400 °C for 30 min and at 450 °C for 60 min. To prepare the molybdenum, vanadium, and tungsten nanooxides, the precursors $(NH_4)\ 6Mo_7O_{24}$ (ammonium paramolybdate), $NH_4VO_3$ (ammonium metavanadate), and $(NH_4)\ 10W_{12}O_{41}\ 4.5\ H_2O$ (ammonium paratungstate) were used. To obtain $TiO_2-MoO_3$, $TiO_2-V_2O_5$, $TiO_2-WO_3$, $TiO_2-MoO_3-WO_3$, and $TiO_2-MoO_3-V_2O_5$ nanoheterostructures, $(NH_4)\ 6Mo_7O_{24}$, $NH_4VO_3$, or $(NH_4)10W_{12}O_{41}$ $4.5\ H_2O$ were dissolved in a mixture of hydrochloric acid and hydrogen peroxide, blended with a doped $TiO_2$ precipitate, and then dried and annealed at 400 °C for 60 min.

Scanning electron microscope JSM7600F (JEOL, Japan) and DRON-4 diffractometer (Burevestnik, Russia) (CuKα radiation) were used to study the structure of the samples. The Scherrer formula was used to determine coherent-scattering-domain sizes (particle sizes) from the full width, at half-maximum of the peaks, and at an instrumental broadening of 0.09°. The BET methodof low-temperature nitrogen adsorption was used to determine the specific surface area, (Chemisorb 2750 instrument, Micromeritics). Diffuse reflection and fluorescence spectra were recorded using an LS-55 Perkin Elmer spectrometer (with spectral range 200–900 nm). The oxidizing power (photocatalytic activity) of the samples was investigated with the reaction of rhodamine dye photodegradation. The dye was applied to the sample surface from aqueous and ethanol solutions. The solvent was dried off carefully. A YG-16 glass filter was used to obtain the illumination in the visible spectral range (from 450 to 750 nm) for the photocatalysis study. Changes in the surface concentration of the dye were monitored according to the diffuse reflectance R value, at a wavelength of the maximum light absorption by the adsorbed dye. The diffuse reflectance was recalculated to the dye molecules surface concentration using Kubelka–Munk approach [21]. The electron spin resonance (ESR) spectrometer (ELEXSYS-E500, Bruker, Germany) was used for the study of radical properties in the prepared samples.

## 3. Results

Micrographs of $TiO_2$-based nanoheterostructures are shown at Figure 1. The figure shows that, in general, the micrographs of different samples have a certain similarity: all the studied structures are nanoparticles grouped into agglomerates of an asymmetric form.

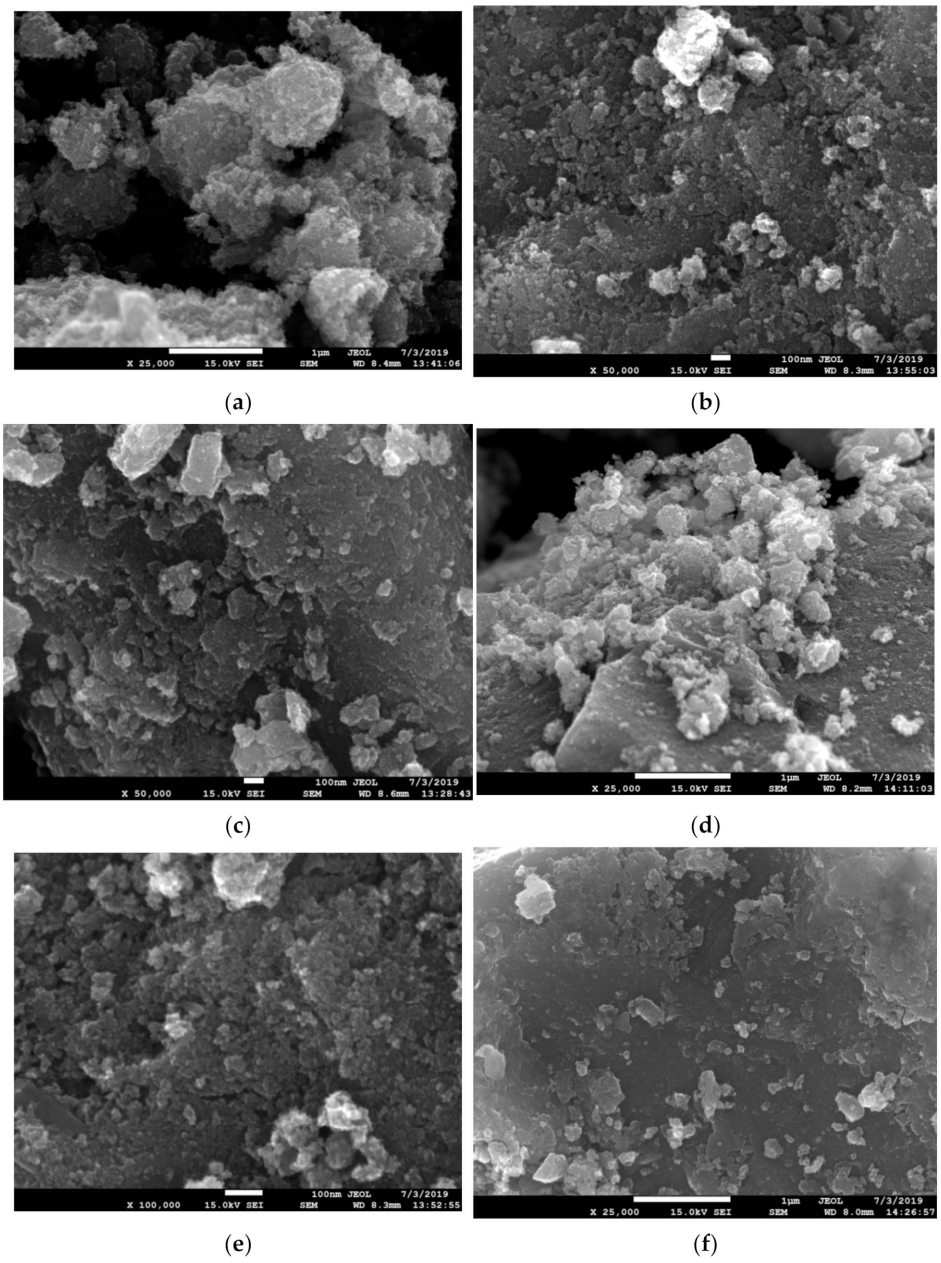


(**a**) (**b**) (**c**) (**d**) (**e**) (**f**)

**Figure 1.** Micrographs of the N-doped $TiO_2$ (**a**), $TiO_2-V_2O_5$ (**b**), $TiO_2-MoO_3$ (**c**), $TiO_2-WO_3$ (**d**), $TiO_2-MoO_3-V_2O_5$ (**e**), and $TiO_2-MoO_3-WO_3$ (**f**) nanoheterostructures. The scale bar's length is 100 nm.

The size of the nanoparticles and their specific surface area were determined from X-ray diffraction (XRD) and low-temperature nitrogen adsorption (BET) data, respectively. The results of these measurements for $TiO_2$ nanoparticles are presented as an example in Table 1.

**Table 1.** $TiO_2$ nanoparticles' average diameter *d* in the nanoheterostructures, calculated using the Scherrer formula from the corresponding reflections broadening and the specific surface area *S*.

| Sample | *d*, nm | *S*, $m^2/g$ |
|---|---|---|
| $TiO_2$ | 14 | 90 |
| $TiO_2/WO_3$ | 9 | 98 |
| $TiO_2/MoO_3/WO_3$ | 4 | 100 |
| $TiO_2/MoO_3$ | 4 | 110 |
| $TiO_2/MoO_3/V_2O_5$ | 9 | 95 |

We have carefully investigated, in another work [20], photocatalysis on the structures prepared by the same method as that used in the present work. The highest rate of photocatalysis in the visible spectral region was observed in the $TiO_2-MoO_3-V_2O_5$ and $TiO_2-MoO_3-WO_3$ nanoheterostructures. As it was revealed in [20], this is due to the higher concentrations of radicals in these structures. After the morphology and structure studies, we repeated part of the photocatalysis measurements with a new batch of samples in the current study. The brief results of the photocatalytic activity of the new samples are presented at Figure 2. The lower is the residual dye concentration $C/C_0$ after the sample exposition to the visible light – the higher is the sample photocatalytic activity. Our new results are very consistent with our previous findings, which allows us to declare a good replicability of the synthesis method and material properties.

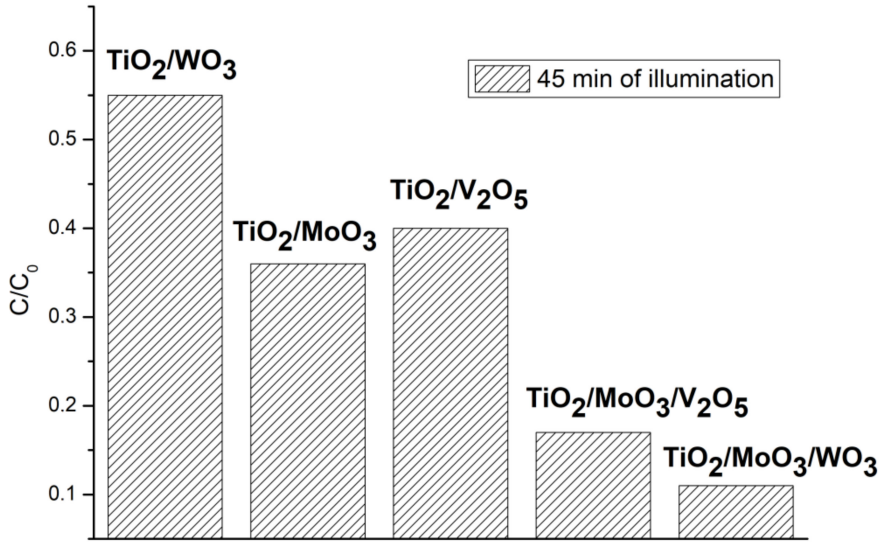


**Figure 2.** Relative rhodamine dye concentration $C/C_0$ at the surface of the studied nanoheterostructures after 45 min of illumination by visible light (in the range 450–750 nm). $C_0$ is initial dye concentration.

Kinetic curves of photocatalysis for $MoO_3$ and $TiO_2$ nanooxides, as well as for nanoheterostructures $TiO_2-WO_3$, $TiO_2-MoO_3$, $TiO_2-MoO_3-V_2O_5$, and $TiO_2-MoO_3-WO_3$ under photoexcitation in the visible spectral region (450–750 nm) are shown in Figure S2 of our Supplementary Materials. We have found that, because of asymmetric charge separation in nanoheterostructures, catalysis lasts on their surface long after light is extinguished.

Since defects at the semiconductors' surface actively interacts with photoexcited charge carriers, we studied the prepared samples by the ESR method. ESR spectra of the previous batch of nanoheterostructures, $TiO_2-MoO_3-V_2O_5$, $TiO_2-MoO_3-WO_3$, $TiO_2-WO_3$, $TiO_2-V_2O_5$, $TiO_2-MoO_3$, and their analyses can be found in Figure S1 of our Supplementary Material. In the investigated samples, an anticorrelation was found between the residual concentration (after photocatalysis) of the test dye and the concentration of radicals in

the nanoheterostructures. Another correlation was found between light absorption in the visible region, the concentration of radicals and the photocatalytic activity [20].

To determine the position of the radicals' energy levels in the band gaps of the used samples, we have applied our original method, developed earlier, which is based on ESR spectroscopy [12]. The dependence of the ESR signal intensity on the photon energy ($h\nu$) was measured when the samples were illuminated directly in the cavity of the spectrometer. A BRUKER ELEXSYS ER 202 UV high-pressure mercury lamp ($\Delta\lambda = 270 - 1000$ nm, 50 W power), equipped with the diffraction monochromator, was used for this purpose. The light intensity was approximately 40 mW $cm^{-2}$.

The study was performed for the nanoheterostructures $TiO_2-MoO_3$, $TiO_2-WO_3$, $TiO_2-V_2O_5$, $TiO_2-MoO_3-WO_3$, $TiO_2-MoO_3-V_2O_5$. The change in the magnitude of the ESR signal of their radicals occurs when a certain energy of the incident photons is reached (specific for each type of radical). It is a very important observation, meaning that, under illumination, defects absorb light and defect recharging occurs. We have found that the increase of the ESR signal in $TiO_2$, for nitrogen radicals, occurs at the photon energy $h\nu \geq 1.5$ eV, i.e., starting from this energy, the electron moves from the radical level to the $TiO_2$ conduction band as a result of light absorption by the dopant. This allows us to estimate the position of this defect level in the band gap of $TiO_2$, as separated from the bottom of the conduction band by a value of 1.5 eV. When illumination was used with the quanta energy $h\nu \geq 3.0$ eV an increase in the ESR signal was observed for $Ti^{3+}$ centers that can be explained by the transition of an electron from the valence band to the initially nonparamagnetic centers of the $Ti^{4+}$/oxygen vacancy, which form electron states in the band gap near the bottom of the $TiO_2$ conduction band and are known from literature as «Urbach tails».

In the same way, the observed increase in the ESR signal intensity for the $Mo^{5+}$ centers in $MoO_3$ under $h\nu \geq 2.6$ eV illumination can be attributed to the transition of electrons from the valence band of molybdenum oxide to the originally nonparamagnetic $Mo^{6+}$ centers, which also form electron states near the bottom of the conduction band of $MoO_3$. The ESR signal, increasing for $V^{4+}$ centers in $V_2O_5$ under illumination by $h\nu \geq 2.1$ eV, in turn can be explained by electrons' transition from the valence band of $V_2O_5$ to the initially nonparamagnetic electron states $V^{5+}$, localized near the $V_2O_5$ conduction band's bottom. Thus, it is possible to construct band diagrams for the nanooxides that make up the studied nanoheterostructures (Figure 3).

In this study, as in previous studies, the photocatalytic activity (oxidative capacity) of the nanocatalyst samples was investigated using the photodegradation reaction of the rhodamine dye (as it is described in the Materials and Methods section). To do this, the dye was applied to the surface of the samples from the solution. Measurements were conducted after the samples' drying. The symmetric possibility of transferring the photoexcitation energy from the adsorbed dye molecules to the semiconductor was not taken into account during our previous studies. We have carefully studied the possibility of energy transfer in the other structures, and it is also known from the literature ([22,23] for example). This energy transfer can lead to the formation of additional free charge carriers. These additional charge carriers may in turn increase photocatalytic efficiency and affect the rhodamine dye's degradation rate. In this way, the photosensitization of semiconductor oxides by dye molecules would promote these dye molecules' faster degradation.

Therefore, in the present work we conducted a special study of the energy transfer efficiency from adsorbed rhodamine-type dye molecules to charge carriers trapped in semiconductor nanoheterostructures possessing photocatalytic activity. For this study, rhodamine dye was adsorbed onto the surface of the photocatalysts' surface at a concentration providing maximal fluorescence intensity. The fluorescence spectra of the rhodamine dye adsorbed on the $TO_2$ surface are shown at Figure 4.

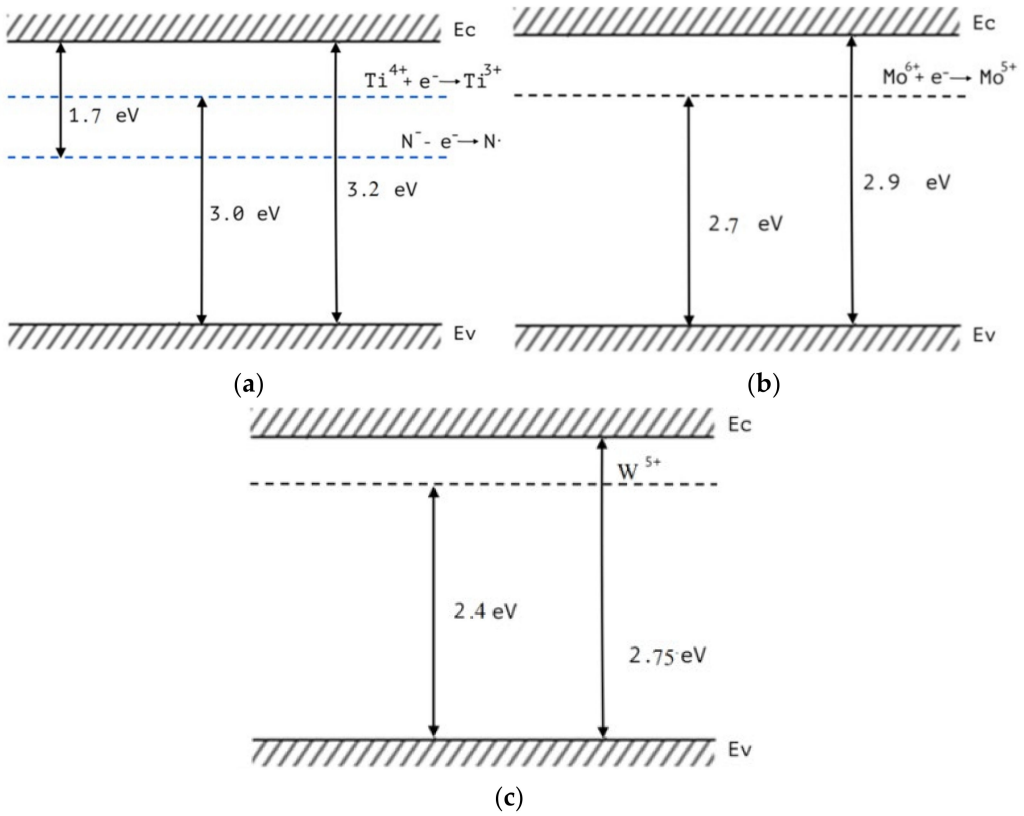


**Figure 3.** Band diagrams of the nanooxides of titanium (**a**), molybdenum (**b**), and tungsten (**c**), combined into $TiO_2$-$MoO_3$-$WO_3$ samples.

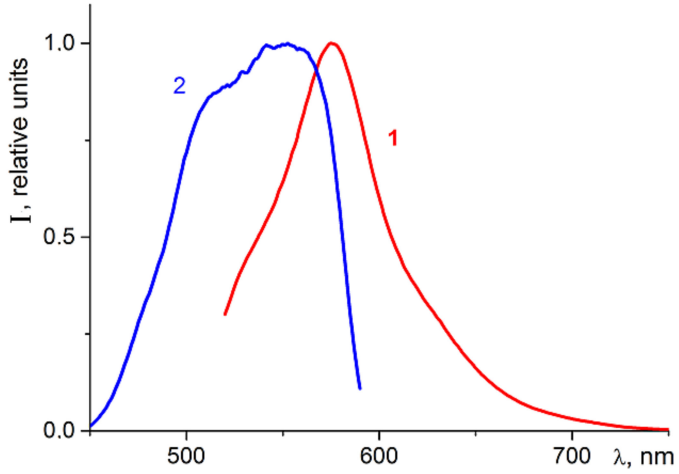


**Figure 4.** The fluorescence spectrum (**1**) and the fluorescence excitation spectrum (**2**) of the rhodamine dye adsorbed on the $TO_2$ surface.

It can be seen from the fluorescence excitation spectrum that the effective excitation of rhodamine molecules does not occur when illuminated at wavelengths shorter than 450 nm.

The remaining research cycle was carried out as follows. For each type of the samples, two series of measurements of the time-intensity dependence I(t) at the fluorescence maximum were performed. The first series of measurements was carried out when the sample was illuminated (between the registrations of the spectra) by radiation at a 333-nm wavelength, outside the effective absorption band of the dye, but in the absorption band of the photocatalysts. The second series was carried out with constant illumination inside the

dye absorption band at a 500-nm wavelength. The fluorescence spectra of the dye were always recorded with excitation at a 500-nm wavelength.

Let us first compare the efficiency of photocatalysis, obtained in symmetric conditions, by measuring the quenching of the dye's fluorescence on different nanoheterostructures when illuminated at the same 333-nm wavelength.

The time dependencies of the maximum fluorescence intensity of rhodamine dye molecules adsorbed at the photocatalysts surface are shown at Figure 5. The curves reflect the time dependence of the fluorescence intensity of the adsorbed dye when the structures were illuminated at a 333-nm wavelength between short runs of fluorescence measurements. The graphs show that the luminescence-quenching rate of $TiO_2$–$MoO_3$–$WO_3$ exceeds the result for $TiO_2$–$WO_3$ and very significantly exceeds the quenching rate obtained for $TiO_2$. This corresponds to our data (obtained by an independent method) on the rate of photocatalysis on these structures. Thus, it becomes clear that both methods are symmetric and it is possible to estimate the rate of photocatalysis by quenching the luminescence of adsorbed organic dyes.

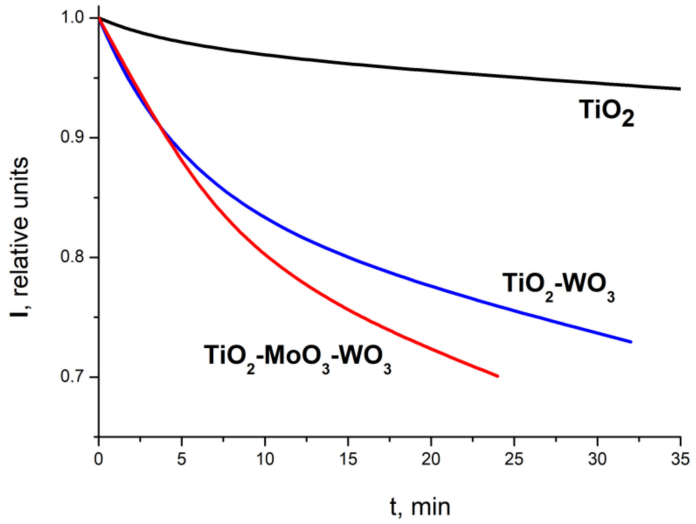


**Figure 5.** Time dependencies of the maximum fluorescence intensity of rhodamine dye molecules adsorbed at photocatalysts' surface (333-nm excitation between the fluorescence measurements).

Let us now compare the symmetric photocatalysis results obtained by illumination at two different wavelengths. The results for $TiO_2$ are shown in Figure 6a. As it is known, rhodamine dye is able to transfer photoexcitation energy to a semiconductor, leading to the release of charge carriers from the traps to the conduction band [22,23]. Probably, this process is very effective in the $TiO_2$–rhodamine system.

As a result, despite the relatively low illumination intensity, the photocatalytic destruction of the dye molecules leads to a noticeable quenching of the fluorescence over time. The efficiency of the process for $TiO_2$ is asymmetric; under illumination in the dye absorption band it is significantly higher than that under ultraviolet illumination.

The Figure 6b shows that green light illumination (500 nm) in the dye-absorption band practically does not lead to degradation of rhodamine molecules adsorbed on nanoheterostructures $TiO_2$–$WO_3$, while ultraviolet illumination leads to a fairly rapid degradation of the dye. It should be noted that the initial fluorescence intensity of rhodamine on the surface of $TiO_2$–$WO_3$ structures was 5–7 times lower than on $TiO_2$, despite their same dye concentrations. Such a significant quenching (right after the dye deposition) of luminescence most likely indicates a noticeable energy transfer from the dye to the semiconductor. However, this does not lead to additional degradation of the dye over time when the structure is illuminated at the wavelength of 500 nm.

The time dependencies of the fluorescence intensity of rhodamine dye on the $TiO_2$–$MoO_3$–$WO_3$ surface, under illumination at 500-nm and 333-nm wavelengths, are shown in Figure 6c. The initial fluorescence intensity of rhodamine dye on the surface of these structures was 5–7 times lower than that on the $TiO_2$ surface, the same as in the previous case. When the structure was illuminated at a 500-nm wavelength, the degradation of the dye fluorescence was observed to be approximately twice slower than on the $TiO_2$ surface—and, when illuminated at the wavelength of 333 nm, the rate of the dye degradation was quite high.

The initial fluorescence intensity of rhodamine at the surface of $TiO_2$–$MoO_3$ samples was approximately 20 times lower than that for the $TiO_2$ surface, and it practically did not change during irradiation at the wavelengths of 500 and 333 nm. At the same time, the dye fluorescence maximum was shifted by 10 nm to the short-wave region, as compared with the rest of the samples. This may indicate a strong bonding between the dye molecules and the substrate for $TiO_2$–$MoO_3$ structures. The similar significant shift in the emission spectrum of rhodamine molecules is usually observed in the presence of strong local electric fields of negatively charged particles near the adsorbed molecules [24]. It is possible that the observed luminescence of the dye is associated with those of its molecules that were adsorbed far from the active centers on the surface of the catalyst, and that those dye molecules that were located close to the active centers experienced the action of the latter and did not contribute to the luminescence.

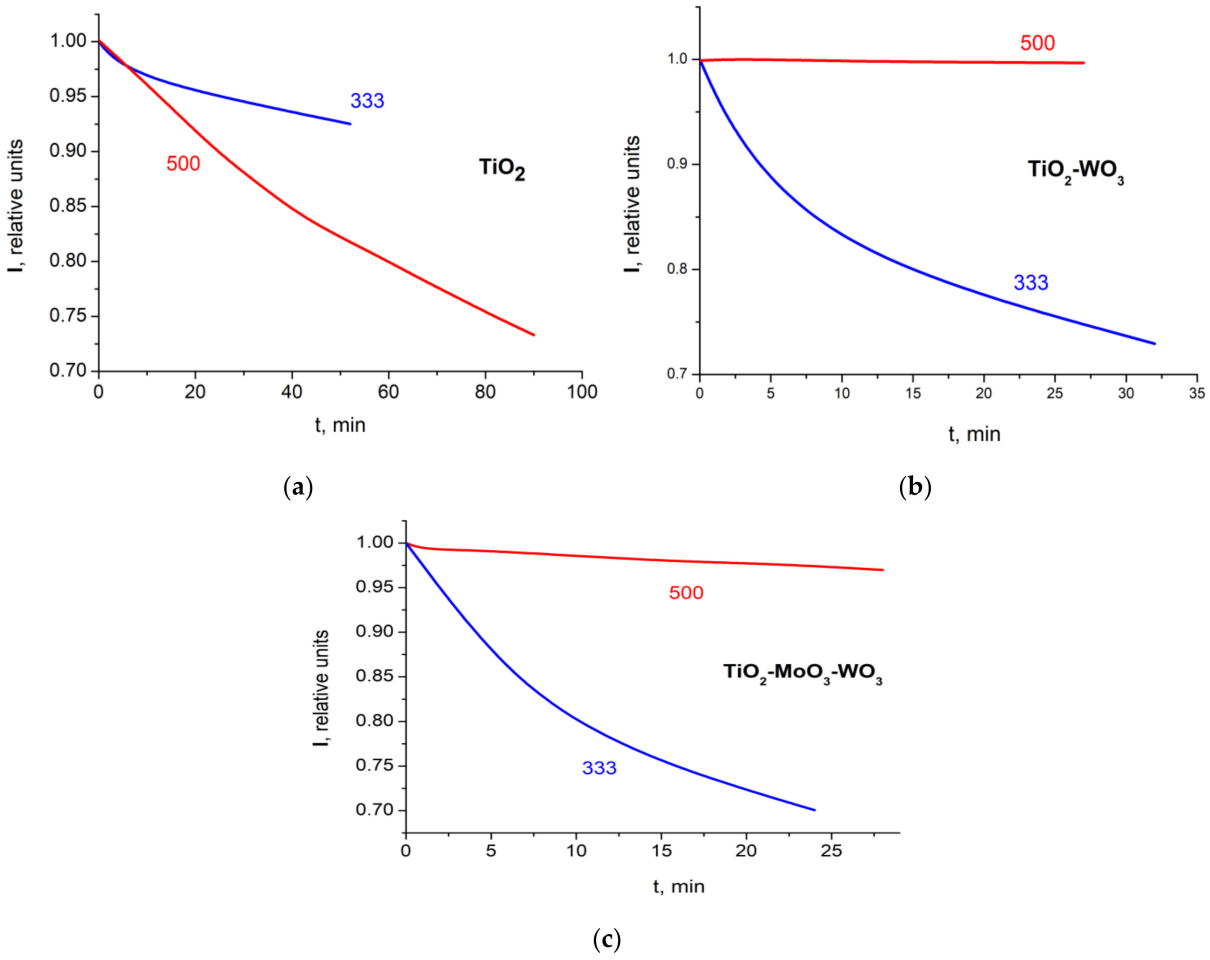


**Figure 6.** Time dependencies of the maximum fluorescence intensity of rhodamine dye molecules adsorbed at the surface of photocatalysts $TiO_2$ (**a**), $TiO_2$–$WO_3$ (**b**) and $TiO_2$–$MoO_3$–$WO_3$ (**c**) under the conditions of 333-nm and 500-nm illumination between the fluorescence measurements.

At the surfaces of the $TiO_2$–$V_2O_5$ and $TiO_2$–$MoO_3$–$V_2O_5$ samples, the initial fluorescence intensity of rhodamine dye was lower than the equipment noise level, which indicates an exceptionally strong quenching (similar to what we have previously observed for vanadium oxides [25]).

The explanation of the catalysis results obtained by illumination at the 500-nm wavelength can be obtained by comparing them with the absorption spectra of the studied nanoheterostructures in the visible region. To do this, we considered the difference of absorption spectra in the visible region between the studied nanoheterostructures and pure nanocrystalline $TiO_2$. The heterostructures used in this study were produced on the basis of N-doped $TiO_2$. The difference absorption spectrum for N-doped $TiO_2$ is represented at Figure 7a. Such doping creates an additional wide, structureless absorption band for titanium dioxide nanocrystals, from about 420 to 720 nm. This may correspond to a fairly uniform spectrum of electronic states in the band gap of $TiO_2$. Therefore, the adsorbed molecules of the rhodamine dye (when illuminated at 500 nm) can efficiently transfer the photoexcitation energy on the order of 2.16 eV (≈575 nm, see Figure 4) to the semiconductor via the induction-resonance symmetric dipole–dipole mechanism. Using this energy, the electrons are effectively ejected from the local states in the band gap to the conduction band of $TiO_2$. This can lead to the accelerated photodegradation of the dye on the surface of nitrogen-doped titanium dioxide when illuminated at a 500-nm wavelength. In addition, the doped material of the photocatalyst itself absorbs radiation at the wavelength of 500 nm (used for the measurement), which can also lead to the observed effect.

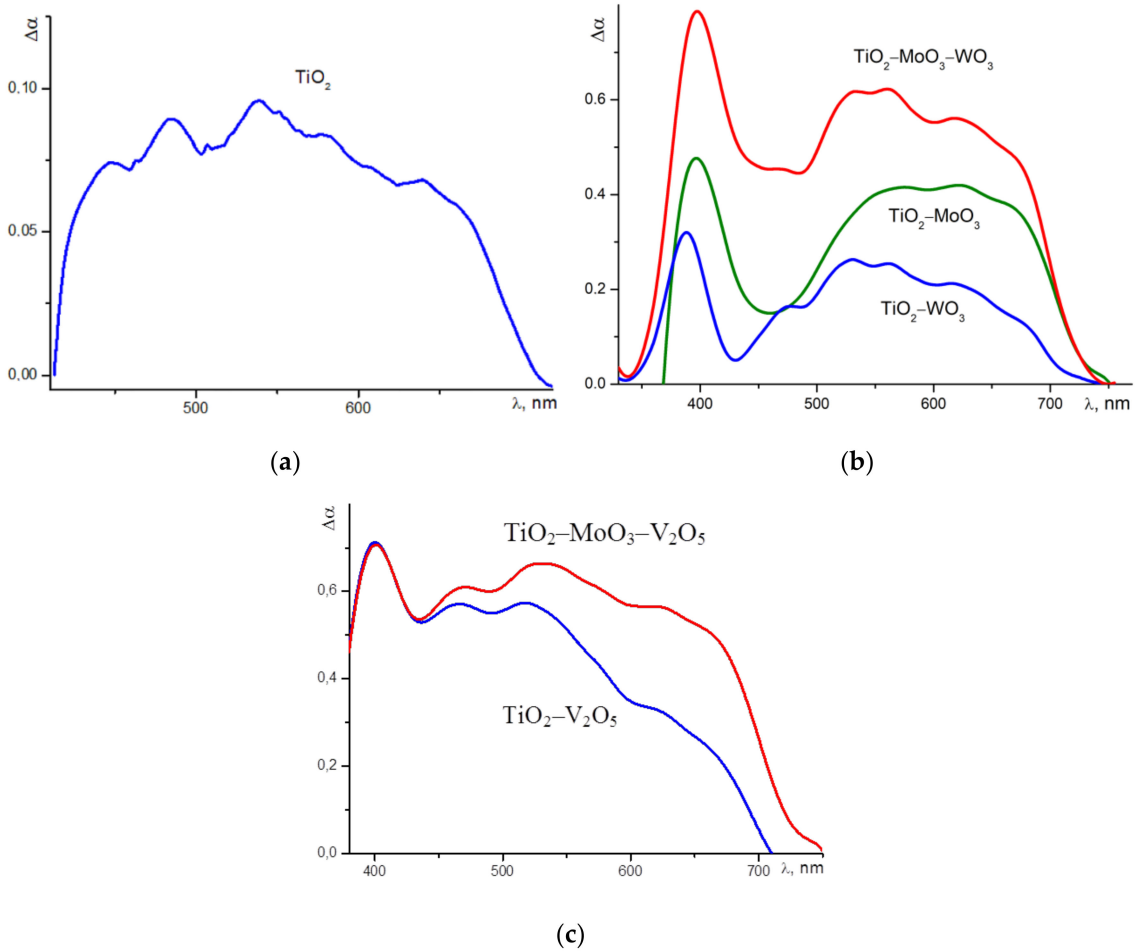


**Figure 7.** The difference of the absorption spectra in the visible region of nanocrystalline N-doped $TiO_2$ (**a**); $TiO_2$–$WO_3$, $TiO_2$–$MoO_3$, $TiO_2$–$MoO_3$–$WO_3$ (**b**) and $TiO_2$–$V_2O_5$, $TiO_2$–$MoO_3$–$V_2O_5$ (**c**) and the absorption of pure titanium dioxide.

Samples of $TiO_2$–$WO_3$, $TiO_2$–$MoO_3$ and $TiO_2$–$MoO_3$–$WO_3$ more effectively absorb light in the visible region than N-doped $TiO_2$. The difference between the absorption spectra of these nanoheterostructures and pure titanium dioxide in the visible region is shown at Figure 7b, but there is a clear dip in their absorption spectra in the range of 420 to 540 nm. Therefore, the illumination of such samples at a 500-nm wavelength should not lead to a significant photocatalytic effect. Although all three of these structures can effectively absorb radiation with the wavelength of ~575 nm, this means that in their electronic spectrum there are states that could be acceptors for non-radiative energy transfer from the dye molecules. Moreover, the $TiO_2$–$MoO_3$–$WO_3$ nanoheterostructures have symmetric behaviour regarding their absorption coefficients and photocatalysis. These samples have a higher absorption coefficient at the 500-nm wavelength than the other two structures (Figure 7b), and their photocatalysis is more effective under such illumination (Figure 2).

Thus, we were able to show that under the illumination of nanoheterostructures with adsorbed rhodamine dye, at the dye-absorption wavelength (500 nm), photocatalytic reactions are mainly determined by the absorption of light by the nanostructures themselves, and not by the transfer of energy from the dye. Since a strong quenching of the initial fluorescence is observed on the surface of all studied nanoheterostructures, it can be stated that the nonradiative energy transfer from the dye molecules associated with such quenching occurs, but does not lead to a significant additional acceleration of photocatalysis. This means that the determination of the photocatalytic efficiency under illumination in the visible range, using adsorbed rhodamine-type dyes, is a valid procedure.

As for photocatalysis with the use of $TiO_2$–$V_2O_5$ and $TiO_2$–$MoO_3$–$V_2O_5$ nanoheterostructures, their absorption in the visible region is very intense and does not have a noticeable dip (Figure 7c). In addition, the quenching of the dye luminescence on the surfaces of these structures was so strong that it was not possible to measure the kinetics.

## 4. Conclusions

The photocatalysts $TiO_2-MoO_3$, $TiO_2-V_2O_5$, $TiO_2-WO_3$, $TiO_2-MoO_3-WO_3$, and $TiO_2-MoO_3-V_2O_5$, with high activity in visible range, were synthesized and studied using microscopy, XRD, ESR and optical techniques. Using the ESR method, the energy position of the different radicals in the band gap of nanooxides was determined and their ability to absorb visible light by radicals has been demonstrated. We have performed, for the first time, a symmetric study of the luminescence of dye molecules adsorbed by nanoheterostructures' surfaces and these structures' catalytic activity. We have shown that, under the illumination of nanoheterostructures with adsorbed rhodamine dye at the dye absorption wavelength (500 nm), photocatalytic reactions are mainly determined by light absorption by the nanostructures themselves, and not by energy transfer from the dye. This important result shows that the high photocatalytic activity of photocatalysts with symmetric crystal structures is the primary criterion for the creation of energy-efficient photocatalysts. We have also proved that the method of catalytic activity measurement, using adsorbed dye, is valid. The prepared nanoheterostructures, based on titanium, molybdenum, tungsten, and vanadium nanooxides with high radical concentrations and high rates of photocatalysis, can be used to create energy-efficient photocatalytic devices operating under periodic illumination in the visible range of the spectrum.

**Supplementary Materials:** The following are available online at https://www.mdpi.com/article/10.3390/sym13091758/s1, Figure S1: ESR spectra of nanoheterostructures $TiO_2-WO_3$ (1), $TiO_2-V_2O_5$ (2), $TiO_2-MoO_3$ (3), $TiO_2-MoO_3-V_2O_5$ (4), $TiO_2-MoO_3-WO_3$ (5), Figure S2: Kinetic curves of photocatalysis for $MoO_3$ (1a) and $TiO_2$ (1b) nanooxides, and nanoheterostructures $TiO_2-WO_3$ (2), $TiO_2-MoO_3$ (3), $TiO_2-MoO_3-V_2O_5$ (4), and $TiO_2-MoO_3-WO_3$ (5) under photoexcitation in the visible spectral region (450–750 nm). Arrows show the moments of switching illumination on (t = 0) and off (t = 20 min). $C_0$ is the initial dye concentration at the moment t = 0 and C is the dye concentration at the moment t. $TiO_2$ doped with nitrogen was used.

**Author Contributions:** Conceptualization, E.K. and V.Z.; methodology, investigation E.K., V.Z., A.M. and A.I.; writing—original draft preparation, E.K., V.Z. and A.M.; writing—review and editing, E.K., V.Z. and A.I. All authors have read and agreed to the published version of the manuscript.

**Funding:** The research was carried out with financial support of the Russian Foundation for Basic Research within the framework of research project no. 18-29-23051.

**Institutional Review Board Statement:** Not applicable.

**Informed Consent Statement:** Not applicable.

**Data Availability Statement:** The datasets obtained and analysed during the current study are available from the corresponding author on reasonable request.

**Acknowledgments:** ESR, luminescent and scattering spectroscopy measurements were carried out using equipment of the shared facilities of Moscow State University.

**Conflicts of Interest:** The authors declare no conflict of interest. The funders had no role in the design of the study; in the collection, analyses, or interpretation of data; in the writing of the manuscript, or in the decision to publish the results.

## References

1. O'Regan, B.; Gratzel, M. A low-cost, high-efficiency solar cell based on dye-sensitized colloidal $TiO_2$ films. *Nature* **1991**, *353*, 737–740. [CrossRef]
2. Mills, A.; Le Hunte, S. An overview of semiconductor photocatalysis. *J. Photochem. Photobiol. A* **1997**, *108*, 1–35. [CrossRef]
3. Schneider, J.; Matsuoka, M. Understanding $TiO_2$ photocatalysis: Mechanisms and materials. *Chem. Rev.* **2014**, *114*, 9919–9986. [CrossRef]
4. Sasan, K.; Zuo, F. Self-doped $Ti^{3+}$-$TiO_2$ as a photocatalyst for the reduction of $CO_2$ into a hydrocarbon fuel under visible light irradiation. *Nanoscale* **2015**, *7*, 13369–13372. [CrossRef]
5. Ola, O.; Maroto-Valer, M. Review of material design and reactor engineering on $TiO_2$ photocatalysis for $CO_2$ reduction. *J. Photochem. Photobiol.* **2015**, *24*, 16–42. [CrossRef]
6. Liu, D.; Zi, W.; Sajjad, S.D. Reversible Electron Storage in an All-Vanadium Photoelectrochemical Storage Cell: Synergy between Vanadium Redox and Hybrid Photocatalyst. *ACS Catal.* **2015**, *5*, 2632–2639. [CrossRef]
7. Chen, X.; Mao, S. Titanium dioxide nanomaterials: Synthesis, properties, modifications and applications. *Chem. Rev.* **2007**, *107*, 2891–2959. [CrossRef]
8. Hoffmann, M.R.; Martin, S.T.; Choi, W. Environmental Applications of Semiconductor Photocatalysis. *Chem. Rev.* **1995**, *95*, 69–96. [CrossRef]
9. Fujishima, A.; Rao, T.N.; Tryk, D.A. Titanium dioxide photocatalysis. *J. Photochem. Photobiol. C* **2000**, *1*, 1–21. [CrossRef]
10. Serpone, N.; Pelizzetti, E. *Photocatalysis: Fundamentals and Applications*; Wiley: New York, NY, USA, 1989.
11. Sviridova, T.V.; Sadovskaya, L.Y.; Shchukina, E.M. Nanoengineered thin-film $TiO_2$/h-$MoO_3$ photocatalysts capable to accumulate photoinduced charge. *J. Photochem. Photobiol. A* **2016**, *327*, 44–50. [CrossRef]
12. Konstantinova, E.A.; Minnekhanov, A.A.; Kokorin, A.I.; Sviridova, T.V.; Sviridov, D.V. Determination of the Energy Levels of Paramagnetic Centers in the Band Gap of Nanostructured Oxide Semiconductors Using EPR Spectroscopy. *J. Phys. Chem. C* **2018**, *122*, 10248–10254. [CrossRef]
13. Asahi, R.; Morikawa, T.; Ohwaki, T.; Aoki, K.; Taga, Y. Visible-light photocatalysis in nitrogen-doped titanium oxides. *Science* **2001**, *293*, 269–271. [CrossRef]
14. Rupa, A.V.; Divakar, D.; Sivakumar, T. Titania and noble metals deposited titania catalysts in the photodegradation of tartazine. *Catal. Lett.* **2009**, *132*, 259–267. [CrossRef]
15. Barbieriková, Z.; Pližingrová, E.; Motlochová, M.; Bezdička, P.; Boháček, J.; Dvoranová, D.; Mazúr, M.; Kupčík, J.; Jirkovský, J.; Šubrt, J.; et al. N-Doped titanium dioxide nanosheets: Preparation, characterization and UV/visible-light activity. *Appl. Catal. B Environ.* **2018**, *232*, 397–408. [CrossRef]
16. Miyamoto, N.S.; Miyamoto, R.; Giamello, E.; Kurisaki, T. Characterization and photocatalytic properties of lutetium ion-doped titanium dioxide photocatalyst. *Res. Chem. Intermed.* **2018**, *44*, 4577–4594. [CrossRef]
17. Minnekhanov, A.A.; Le, N.T.; Konstantinova, E.A.; Kashkarov, P.K. Influence of Defects on Photoconductivity and Photocatalytic Activity of Nitrogen-Doped Titania. *Appl. Magn. Reson.* **2017**, *48*, 335–345. [CrossRef]
18. Yan, M.; Li, G.; Guo, C.; Guo, W.; Ding, D.; Zhanga, S.; Liu, S. $WO_{3-x}$ sensitized $TiO_2$ spheres with full-spectrum-driven photocatalytic activities from UV to near infrared. *Nanoscale* **2018**, *8*, 17828–17835. [CrossRef]
19. Skorb, E.V.; Ustinovich, E.A.; Kulak, A.I.; Sviridov, D.V. Photocatalytic activity of $TiO_2$:$In_2O_3$ nanocomposite films towards the degradation of arylmethane and azo dyes. *J. Photochem. Photobiol. A* **2008**, *193*, 97–102. [CrossRef]
20. Konstantinova, E.A.; Zaitsev, V.B.; Kytina, E.V.; Marikutsa, A.V. Photoaccumulating Nanoheterostructures Based on Titanium Dioxide. *Semiconductors* **2021**, *55*, 219–227. [CrossRef]

21. Kortüm, G.; Braun, W.; Herzog, G. Principles and Techniques of Diffuse-Reflectance Spectroscopy. *Angew. Chem. Int. Ed. Engl.* **1963**, *2*, 333–341.
22. Zaitsev, V.; Rosty, R.; Kebbekus, B. The testing of a semiconductor-based adsorption modified photosensitive sensor for its response to a volatile organic compound, oxygen, humidity and temperature. *Sens. Act. B* **2005**, *107*, 347–352. [CrossRef]
23. Li, H.; Devaux, A.; Ruiz, A.Z.; Calzaferri, G. Electronic excitation energy transfer from dye-loaded zeolite L monolayers to a semiconductor. *SPIE Proc.* **2006**, *6195*, 61951G. [CrossRef]
24. Gygax, H.; Rebane, A.; Wild, U.P. Stark effect in dye-doped polymers studied by photochemically accumulated photon echo. *J. Opt. Soc. Am. B* **1993**, *10*, 1149–1158. [CrossRef]
25. Zaitsev, V.B.; Kiselev, V.F.; Levshin, N.L.; Plotnikov, G.S. Effect of adsorbed photo-excited dye molecules on the semiconductor metal phase-transition. *Doklady Akad. Nauk. SSSR* **1989**, *304*, 649–652.